Pergamon

0301-9322(94)00041-7

Int. J. Multiphase Flow Vol. 20, No. 6, pp. 1053–1070, 1994

0301-9322/94 $7.00 + 0.00

NUMERICAL SIMULATION OF CIRCULATION IN GAS–LIQUID COLUMN REACTORS: ISOTHERMAL, BUBBLY, LAMINAR FLOW

I. CELIK and Y.-Z. WANG

Department of Mechanical and Aerospace Engineering, West Virginia University, Morgantown, WV 26506-6101, U.S.A.

(Received 3 June 1992; in revised form 26 April 1994)

Abstract—The gas–liquid flow inside a circular, isothermal column reactor with a vertical axis has been studied using numerical simulations. The flow is assumed to be in the laminar, bubbly flow regime which is characterized by a suspension of discrete air bubbles in a continuous liquid phase such as glycerol water. The mathematical formulation is based on the conservation of mass and momentum principle for the liquid phase. The gas velocity distribution is calculated via an empirically prescribed relative velocity as a function of void fraction. The interface viscous drag forces are prescribed empirically. For some cases a profile shape is assumed for the void ratio distribution. The influence of various profile shapes is investigated. The results are compared with those where the void ratio distribution is calculated from the conservation of mass equation. The mathematical model has been implemented by modifying a readily available computer code for single-phase newtonian fluid flows. The numerical discretization is based on a finite volume approach. The predictions show a good agreement with measurements. The circulation pattern seems not to be so sensitive to the actual shape of the void fraction profiles, but the inlet distribution of it is important. A significantly different flow pattern results when the void fraction distribution is calculated from the transport equation, as compared to those with *a priori* prescribed profiles. When the void fraction is uniformly distributed over the whole distributor plate, no circulation is observed. Calculations also show that even the two-phase systems with a few discrete bubbles can be simulated successfully by a continuum model.

Key Words: numerical modeling, column reactors, gas–liquid flow, two-phase flow, circulation, void fraction distribution

1. INTRODUCTION

The study of the circulation patterns inside a column reactor is of theoretical and practical significance, because of their wide use in the industry as chemical or biochemical reactors. Bubble column reactors offer several advantages over conventional fixed bed reactors, e.g. in Fischer–Tropsch slurry reactors lower hydrogen-to-monoxide ratios can be tolerated and hot-spots are controlled in the bed so that catalyst deactivation is reduced. The gas may be introduced evenly through a distributor plate into the slurry, so the circulation pattern of continuous liquid phase can be controlled (Clark *et al.* 1990a).

Numerous mathematical models are available in the literature for calculation of relevant parameters such as the gas hold-up (i.e. volume fraction of the gas phase), the liquid velocity and the size and strength of the liquid circulation cells. Freedman & Davidson (1969), Rietema & Ottengraf (1970) and Hills (1974) have reported on approximate models based on pressure balance to calculate liquid circulation velocity. Whalley & Davidson (1974) have shown that their model, based on the energy balance, predicted liquid circulation velocities which are in better agreement with experiments than those obtained from the models based on pressure balance. Joshi & Sharma (1979) have adapted the energy balance method and reported good agreement between their calculations and experiments for the values of the liquid velocity and void fraction. Clark *et al.* (1987, 1990b) have reviewed the so called "drift flux models" and presented their improved version. Rice & Geary (1990) also proposed a model for turbulent flow in viscous bubble columns where they prescribe *a priori* the void fraction, ϵ, profiles empirically. They showed that the c profile parameter, m, can change an order of magnitude, and it had to be prescribed empirically. Most of these models use primarily empirical relations which relate the superficial gas and liquid velocities

to the average void fraction. Clark *et al.* (1990b) suggested an approximate model to predict the empirical constant in one of these models, and also found that it varied significantly as a function of Froude number and Galileo number. Their conclusion was "that a direct drift-flux approach is not suitable unless the void fraction distribution is known and that buoyancy effects are insignificant." A further restriction in these models is that the size and the location of the recirculation zone must be assumed *a priori*. For example, in the model proposed by Clark *et al.* (1990b), two zones are identified, namely a central zone where only axial flow is assumed, and a lower zone where only radial flow is assumed. Such assumptions, which are inherent to most approximate models neglect the possibility of multiple circulation cells. To eliminate such restrictive assumptions, it is necessary to develop more rigorous computational fluid flow analysis with which the circulation and the void fraction distribution can be predicted. However such comprehensive numerical simulations of gas–liquid two-phase flow systems are lacking in the literature. This is not surprising in view of the fact that the mathematical formulation for multiphase flows is still in a stage of development. There is no definite form of the governing equations which is generally accepted (for a review, see for example, Stewart & Wendroff 1984). Other difficulties such as handling of interaction terms (interface conditions), the boundary conditions for the dispersed phase and interphase instabilities, make comprehensive numerical modeling a challenging research area and it calls for more attention from the computational fluid dynamicists.

A recent paper by Antal *et al.* (1991) shows clearly how complicated a two-phase flow continuum model can be, even for the simplest flow situation of a fully developed flow in a vertical pipe. These authors present a detailed description of the lateral forces acting on the bubbles and demonstrate their importance. The flow situation in gas–slurry column reactors where there is usually multiple recirculation zones and a free surface bounding the flow, is distinctly different than that in a fully developed pipe flow where the flow is predominantly unidirectional. Hence not all of the assumptions made by Antal *et al.* (1991) are applicable to our case.

This paper reports on the results of a study where the flow and the circulation patterns inside an isothermal column reactor model, in bubbly flow regime, have been simulated numerically. As a first step, only the equation of motion and continuity for the continuous phase have been solved. The gas velocity field is prescribed empirically. The void fraction is either calculated from the transport equation or profile shapes assumed. Only the laminar, bubbly flow regime is considered. This is done to avoid the complexities of a turbulence closure model at higher superficial gas velocities. The possible effects that may arise from the bubble induced pseudo-turbulence (see e.g. Celik & Gel 1993; O'Brien *et al.* 1993) are not included either. To minimize these effects we selected for this study, experimental cases where viscous fluids were utilized with the idea that the fluctuations caused by the passage of bubbles would be damped out and the results would not be significantly affected by the additional correlation terms.

Our model eliminates many of the crude assumptions introduced in previous studies, such as those by Clark *et al.* (1987, 1990b), Durst *et al.* (1984), and Rice & Geary (1990), but at the same time it retains the desired simplicity. The present model is fairly simple, e.g. compared to that of Antal *et al.* (1991), but it contains the primary physical mechanisms to predict circulation patterns in gas–liquid column reactors.

2. MATHEMATICAL MODEL

Governing equations

The mathematical model is based upon the conservation of mass and momentum for the liquid and gas phases including appropriate interface momentum exchange terms. Invoking continuum assumptions and performing a space or time averaging over a macroscopic control volume (see e.g. Anderson & Jackson 1967; Homsy 1983; Drew 1983), these equations can be written in cylindrical coordinates (for more details, see Clark *et al.* 1990 and Celik & Wang 1990; see also appendix A) as:

Continuity

$$\frac{\partial}{\partial x}(\rho_l u_L) + \frac{1}{r}\frac{\partial}{\partial r}(r\rho_l v_L) = 0 \qquad [1]$$

x-Momentum

$$\frac{\partial}{\partial x}(\rho_l u_L u_L)+\frac{1}{r}\frac{\partial}{\partial r}(r\rho_l u_L v_L)=-(1-\epsilon)\frac{\partial P}{\partial x}-\rho_L g+F_{GL}(u_G-u_L)$$
$$+\frac{\partial}{\partial x}\left(\mu_L\frac{\partial u_L}{\partial x}\right)+\frac{1}{r}\frac{\partial}{\partial r}\left(r\mu_L\frac{\partial u_L}{\partial r}\right)+\frac{\partial}{\partial x}\left(\mu_L\frac{\partial u_L}{\partial x}\right)+\frac{1}{r}\frac{\partial}{\partial r}\left(r\mu_L\frac{\partial v_L}{\partial x}\right) \quad [2]$$

r-Momentum

$$\frac{\partial}{\partial x}(\rho_l u_L v_L)+\frac{1}{r}\frac{\partial}{\partial r}(r\rho_l v_L v_L)=-(1-\epsilon)\frac{\partial P}{\partial r}+F_{GL}(v_G-v_L)$$
$$+\frac{\partial}{\partial x}\left(\mu_L\frac{\partial v_L}{\partial x}\right)+\frac{1}{r}\frac{\partial}{\partial r}\left(r\mu_L\frac{\partial v_L}{\partial r}\right)+\frac{1}{r}\frac{\partial}{\partial r}\left(r\mu_L\frac{\partial v_L}{\partial r}\right)+\frac{\partial}{\partial x}\left(\mu_L\frac{\partial u_L}{\partial r}\right)-\mu_L\frac{2v_L}{r^2} \quad [3]$$

where the subscripts L and G denote the liquid phase and gas phase, respectively; ϵ is the void fraction (i.e. volume concentration of gas), $\rho_l=(1-\epsilon)\rho_L$, $\rho_2=\epsilon\rho_G$ are the macroscopic densities, ρ_L and ρ_G being the microscopic liquid and gas densities, respectively; u and v are the liquid and gas velocities in the x- and r- directions, respectively; g is the acceleration of gravity, μ_L is the liquid viscosity, P is the pressure and F_{GL} is the momentum exchange function between the gas phase and liquid phase. The equations for the gas phase can be obtained from [1]–[3] by changing $(1-\epsilon)$ to ϵ and the subscript "L" to "G".

The last two viscous terms on the right-hand side of [2] and [3] do not normally appear in Navier–Stokes equations for an incompressible, newtonian fluid. But because of the non-zero gradient of the void fraction the fluid acts as a pseudo-compressible fluid and this results in the above-mentioned terms. A derivation in 2-D cartesian coordinates is presented in appendix A to clarify this point.

The global assumptions involved in deriving [1]–[3] are: isothermal, steady, axisymmetric and incompressible flow without swirl and chemical reactions. Further, it should be noted that the way the pressure gradient terms should be handled in [1]–[3] is a controversial issue. There is considerable debate in the literature (see, for example, Stewart & Wendroff 1984) whether $[(1-\epsilon)\nabla P]$ or $\nabla[(1-\epsilon)P]$ should be used in these equations. Both forms satisfy the condition that when the corresponding momentum equations for the two phases are added, the resulting pressure gradient term must be ∇P. Here, the equal pressures model (Stewart & Wendroff 1984) is adapted, i.e. $P_L=P_G=P$. The surface tension effects are not considered in the present study.

F_{GL} is prescribed empirically (see next section). Equations [1]–[3] when written for both phases constitute a closed set of six differential equations for the six unknowns, namely, ϵ, P, u_L, v_L, u_G and v_G. As a first

$$u_s=f(\epsilon, \mathrm{Re}_b). \quad [4]$$

This explicit form of [4] is discussed later in the text.

Interfacial momentum exchange

The momentum transfer between the different phases takes place via several mechanisms, the most important of which being the viscous drag force resulting from the shear stress at the interface and the form drag due to the pressure distribution on the surface of individual bubbles. Other possible mechanisms for momentum transfer include added mass effect, Magnus effect (due to rotation), pressure gradient and shear rate effects of the surrounding fluid (see for example Hinze 1972). For brevity, only the drag force is considered in the present analysis. The only other force which might be of relevance to the present study is the Saffman lift force which acts in the normal direction to the relative velocity vector, and it is of significance only in the areas with large liquid velocity gradient, e.g. near the walls. Mainly because of the large degree of uncertainty in the magnitude and direction of this force (see e.g. Yamamoto *et al.* 1990), we did not include it in the present calculations. But when there is a reliable empirical formula it can easily be incorporated in the present calculation procedure. The validity of the above assumptions is tested by comparing the calculations with experiments.

Table 1. Coefficients for [6] for air bubbles in "pure systems"†

Re_b range	a	b
0–2	24	1.000
2–10	23.66	0.981
10–100	14.9	0.780
100–1000	6.9	0.613

†"Pure systems" meaning uncontaminated solutions (see Clift *et al.* 1978, for details).

In the bubbly flow regime, the total drag force can be related to that of a single bubble. Hirt (1982) and Harlow & Amsden (1975) suggested a relation for water droplets in steam where they accounted for bubble-to-bubble interaction crudely by multiplying the usual drag relation with an ϵ term. For our problem, ρ_G in the original equation is replaced by ρ_L and ϵ by $(1-\epsilon)$. The relation that we used is:

$$F_{GL} = \frac{3}{4}\epsilon^2(1-\epsilon)\rho_L \frac{|\mathbf{u}_L - \mathbf{u}_G|}{d_p} C_D \qquad [5]$$

where d_p is the droplet diameter and C_D is the drag coefficient for an isolated droplet.

As a first approximation, [5] is used for the bubbly flow regime of this study where C_D is replaced by an empirical relation for bubbles in water. Such a C_D relation can be derived by curve fitting to the experimental data presented by Clift *et al.* (1978). For bubbles in "pure systems", the following function is suggested by us,

$$C_D = a\ \mathrm{Re}_b^{-b} \qquad [6]$$

where Re_b is the bubble Reynolds number defined as

$$\mathrm{Re}_b = \frac{\rho_L |\mathbf{u}_L - \mathbf{u}_G| d_b}{\mu_L}.$$

The coefficients a and b are given in table 1 for different Reynolds number ranges. This particular form is adopted because it simplifies the calculation of relative velocity considerably.

Simplification for the gas phase

Instead of solving for the gas momentum equations, first the gas velocities are determined from an empirical relative velocity relation. For small void ratios (i.e. dilute flow with a dispersed gas phase) the gas velocities in the radial and axial direction can be calculated from

$$v_s = 0 \text{ or } v_L = v_G \qquad [7]$$

$$u_G = u_s + u_L \qquad [8]$$

where the relative velocity, u_s, is given by

$$u_s = U_{b\infty}(1\text{-}\epsilon). \qquad [9]$$

$U_{b\infty}$ is the terminal velocity of an isolated bubble in an infinite liquid medium. The effect of void ratio, ϵ, on the relative velocity as given in [9] is suggested by Wallis (1962). $U_{b\infty}$ can be calculated by equating the drag force to the difference of the buoyancy force and the weight of the bubble. With the drag relation [6] this force balance results in

$$U_{b\infty} = \left[\frac{4}{3a}\frac{(\rho_L - \rho_G)}{\rho_L} g d_b \left(\frac{\rho_L d_b}{\mu_L}\right)^b\right]^{1/(2-b)}. \qquad [10]$$

For example with $b = 1$ and $a = 24$ (i.e. Stokes range) [10] reduces to

$$U_{b\infty} = \frac{1}{18}\frac{(\rho_L - \rho_G)}{\mu_L} g d_b^2. \qquad [11]$$

If the water (or liquid) is not pure, the degree of contamination may have significant influence on $U_{b\infty}$. For such cases, the empirical data presented by Clift *et al.* (1978) can be used. Another

alternative is to use the terminal velocity relations presented by Hewitt (1982, chapter 2) where the terminal velocity of bubbles in clean fluids is expressed as a function of Re_b and the Galileo number

$$\bar{G}_a = \frac{g\mu_L^4}{\rho_L \sigma^3}.$$

Profiles for ϵ distribution

As a further simplification in the present model, $\epsilon(x, r)$ is assumed to vary as $\epsilon = \epsilon_c \epsilon(r)$, and the shape of the $\epsilon(r)$ profile is prescribed empirically. The purpose of this is to investigate the influence of profile shape assumptions usually made in most approximate models. The advantage of prescribing the ϵ profiles instead of determining them from [14] is to eliminate computational uncertainties such as numerical diffusion in solving [14]. Among the various shapes investigated are linear, parabolic and cosine profiles. The cosine profile, for example, is given by

$$\epsilon(x,r) = \begin{cases} 0.5\epsilon_c[1 + \cos(\pi r/r_s)] & r \leqslant r_s \\ 0 & r_s < r \leqslant R \end{cases} \quad [12]$$

where R is the column radius and r_s is the radius of the bubble street as observed from experiments (Rietema & Ottengraf 1970). Both r_s and ϵ_c can be functions of x [see figure 2(b)]. The center line value ϵ_c is determined from

$$Q_a = 2\pi \int_0^R \epsilon(r) u_G(x,r) r \, dr \quad [13]$$

to ensure continuity for the gas phase. Hence, only the shape of the ϵ profile is assumed *a priori*, but the actual magnitude is calculated as part of the solution. Calculations are also performed where $\epsilon(x, r)$ is calculated from the conservation of mass equation for the gas phase, i.e.

$$\frac{\partial}{\partial x}(\epsilon u_G) + \frac{1}{r}\frac{\partial}{\partial r}(\epsilon r v_G) = 0. \quad [14]$$

Equation [14] is the counterpart of [1] written for the gas phase, i.e. in [1] $\rho_L(1-\epsilon) = \rho_1$ is replaced by $\rho_G \epsilon = \rho_2$ u_L is replaced by u_G and v_L is replaced by v_G; when ρ_G = constant it cancels out.

3. NUMERICAL METHOD

The form of the equations for the continuous liquid phase ([2] and [3]) is amenable for using the finite volume technique (e.g. Patankar 1980) which has been successfully used for the solution of steady, incompressible, single-phase, recirculating flow problems. This formulation takes into account density variation (say due to buoyancy effects) in space which is suitable for the present problem where the microscopic density is constant but the macroscopic density varies according to $\rho_1 = \rho_L(1-\epsilon)$. The well known "SIMPLE" algorithm (see e.g. Patankar 1980) is employed to calculate the pressure field iteratively. However, modifications have been made to account for the pressure gradient terms $(1-\epsilon)\partial P/\partial x$ and $(1-\epsilon)\partial P/\partial r$, and the additional momentum source terms $F_{GL}(u_G - u_L)$ and $F_{GL}(v_G - v_L)$. These modifications have been incorporated in a readily available computer code, TEACH (Gosman & Ideriah 1976; Durst & Loy 1984) and the modified version has been used for the present calculations.

The "hybrid" difference scheme is used in the formulation. This scheme has the property that it switches from central to upwind differencing for high Peclet numbers ($Pe = \rho_L \Delta x u_L/\mu_L$) for the convective terms; for the diffusive terms, the central differencing is employed at all times. For the present application the maximum Pe had an order of magnitude of 1.0. That is, central differencing is used for most of the flow region. This is an important feature of the method especially for calculating the void fraction distribution from [14] which has no physical diffusion. Since the central differencing is a second-order accurate scheme, it minimizes the numerical diffusion. Equation [14] was solved iteratively using the same numerical technique for solving the general transport equation, e.g. [2]. The right-hand side is set equal to zero by appropriately setting the coefficients, such that

$$\rho_1 = \epsilon, u_L = u_G, v_L = v_G, \mu_L = 0.$$

After the liquid velocity components are calculated via SIMPLE algorithm, the gas velocity components are calculated from [7] and [8]. The initial distribution of ϵ was guessed. Iterations are continued with the global gas continuity [13] is satisfied to a reasonable degree of accuracy, as discussed later. It should be noted that the pressure, P, is calculated iteratively so that the equation of continuity for the liquid phase [1] is implicitly satisfied.

Boundary conditions

No slip condition was enforced for the liquid velocities at the walls and at the air inlet (distributor plate); at the center line ($r = 0$) symmetry conditions were imposed. The free surface was assumed to be undisturbed at which the axial-velocity, u_L, was set equal to zero (i.e. no liquid flux through the surface). The radial velocity, v_L, at the free surface was calculated from the condition $\partial v/\partial x = 0$; this is a somewhat arbitrary condition used as a first approximation since no other information is available on v_L.

Boundary conditions are needed for ϵ when it is calculated from [14]. Since there is no mass flux through the walls $\partial\epsilon/\partial r = 0$ was used at the side walls; the same condition applies at the center line due to symmetry. It should be noted that for some cases $\epsilon = 0$ at the wall may be a valid condition, but it is certainly not general, because when bubbles collide with the wall $\epsilon \neq 0$ but its flux is, i.e. $\partial\epsilon/\partial r = 0$. At the inlet, a uniform distribution $\epsilon = \epsilon_0$ was assumed, and ϵ_0 was estimated from the number of holes on the distributor plate, i.e. $\epsilon_0 = \Sigma A_j/A, j = 1, 2, \ldots, n$, A_j is the area of an individual hole, A is the total cross-sectional area of the inlet, n is the number of the holes. Then from [13] the gas velocity is calculated for a given air flow rate, Q_a.

The ϵ values at the free surface are not needed for the calculations, $\epsilon = 1$ was imposed at the grid points just outside the free surface. The present method uses a staggering grid arrangement in which the velocities are staggered and the scalar quantities are stored at the centers of the main grid cells. The gas velocity at the free surface is calculated from [13] to satisfy continuity once ϵ was determined there (see Clark *et al.* 1990, for particular details).

Convergence and grid independence

To ensure properly converged numerical solutions, not only the total residues of difference equations are checked, but also the net liquid flux across the column cross section, Q_{net} and the maximum relative change in the axial velocity, $\Delta u_{max}/u_{max}$ are tracked. The net liquid volume flux should be zero for the present problem. This is normalized by the recirculated liquid volume, Q_{cir}, given by

$$Q_{cir} = 2\pi \int_0^{r_0} (1-\epsilon) u_L r \, dr = -2\pi \int_{r_0}^{R} (1-\epsilon) u_L r \, dr \qquad [15]$$

where r_0 is the zero crossing point for u_L. After about 300 iterations, both Q_{net}/Q_{cir} and $\Delta u_{max}/u_{max}$ values were less than 10^{-5}. Calculations were continued for another 200 iterations to ensure complete convergence.

Two uniform grid distributions were used, namely a coarse grid of 21×12 ($\Delta x = 4$ cm, $\Delta r = 1$ cm), and a fine grid of 42×23 ($\Delta x = 2$ cm and $\Delta r = 0.5$ cm). The difference in liquid velocity from the coarse grid and fine grid solutions was less than 1%. The fine grid solutions are presented in this paper unless stated otherwise.

4. DESCRIPTION OF CASES STUDIED

The experiments of Rietema & Ottengraf

The numerical study simulated, as closely as possible, the experiments performed by Rietema & Ottengraf (1970) where a laminar liquid circulation and bubble street formation were investigated in a Quickfit glass column. The geometric configuration for the glass column is shown in figure 1. The experimental conditions for the numerically simulated case were: liquid (glycerol–water solution) density $\rho_L = 1153$ kg/m^3, viscosity $\mu_L = 0.35$ kg/m-s, air flow rate $Q_a = 11.4$ cm^3/s, gas hold-up $\epsilon_g = 74$ cm^3, mean bubble diameter $d_b = 0.54$ cm and bubble street diameter $D_s = 10.0$ cm. The glass column had a diameter of 22 cm and a height of 122 cm. Initially the column was filled with the liquid solution up to a depth of 80 cm. If the gas hold-up of 74 cm^3 is added to the liquid

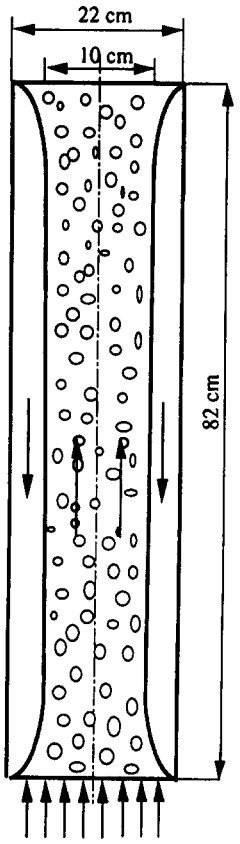

Figure 1. Geometry of the bubble column (experiments by Rietema & Ottengraf, 1970).

volume, the total mixture volume requires a column height of approximately 82 cm. This value was used in the simulations. Air bubbles were formed by means of injection needles. According to experimentors, vertical baffles were placed along the wall, so that a reasonably symmetrical street could be created. The effect of the baffles is not considered in the present study.

For the set of calculations where $\epsilon(x, r)$ is obtained from the solution of [14], a step function $\epsilon = \epsilon_0$ for $r \leqslant r_s$; $\epsilon_0 = 0$ for $r > r_s$, was assumed [see figure 3(b)]. ϵ_0 was approximated as the area fraction of injection holes to the total area. A hole diameter of $0.5\, d_b$ was assumed. r_s/R values were varied between 0.3 and 0.9 to study the influence of distribution at the inlet on the overall circulation patterns.

The experiments of Durst et al.

The numerical simulation for the experiments performed by Durst *et al.* (1984) is accomplished by solving [1]–[3] and [14]; here the ϵ profile is not assumed *a priori*. In this case, a laminar liquid circulation and bubble street formation were investigated in an axisymmetric glass cylinder. The cylinder had an i.d. of 0.1 m. The geometric configuration is shown in figure 4. Two liquid heights $H = 0.098$ m and $H = 0.278$ m were investigated. The liquid (castor oil) properties for the numerically simulated case were: density $\rho_L = 960.3\ \text{kg/m}^3$ and kinematic viscosity $\nu_L = 0.699 \times 10^{-3}\ \text{m}^2/\text{s}$. The bubbles were formed through the nozzle located at the bottom centerline of the cylindrical column. The air was passed through a well-controlled pressure regulator and the resulting bubbles left the nozzle at a steady rate of one every 0.55 s with a diameter d_b of about 5–6.5 mm. A value of $d_b = 6$ mm was used in the numerical simulations.

As boundary conditions for ϵ, at the inlet boundary, a step function $\epsilon = \epsilon_0$ for $r \leqslant r_s$, $\epsilon_0 = 0$ for $r > r_s$, was assumed, where r_s is bubble street radius, which was approximated as the bubble radius of 3 mm. ϵ_0 was determined as the volume fraction of bubbles to the total volume of bubble street between two successively rising bubbles, which resulted in $\epsilon_0 = 0.12$.

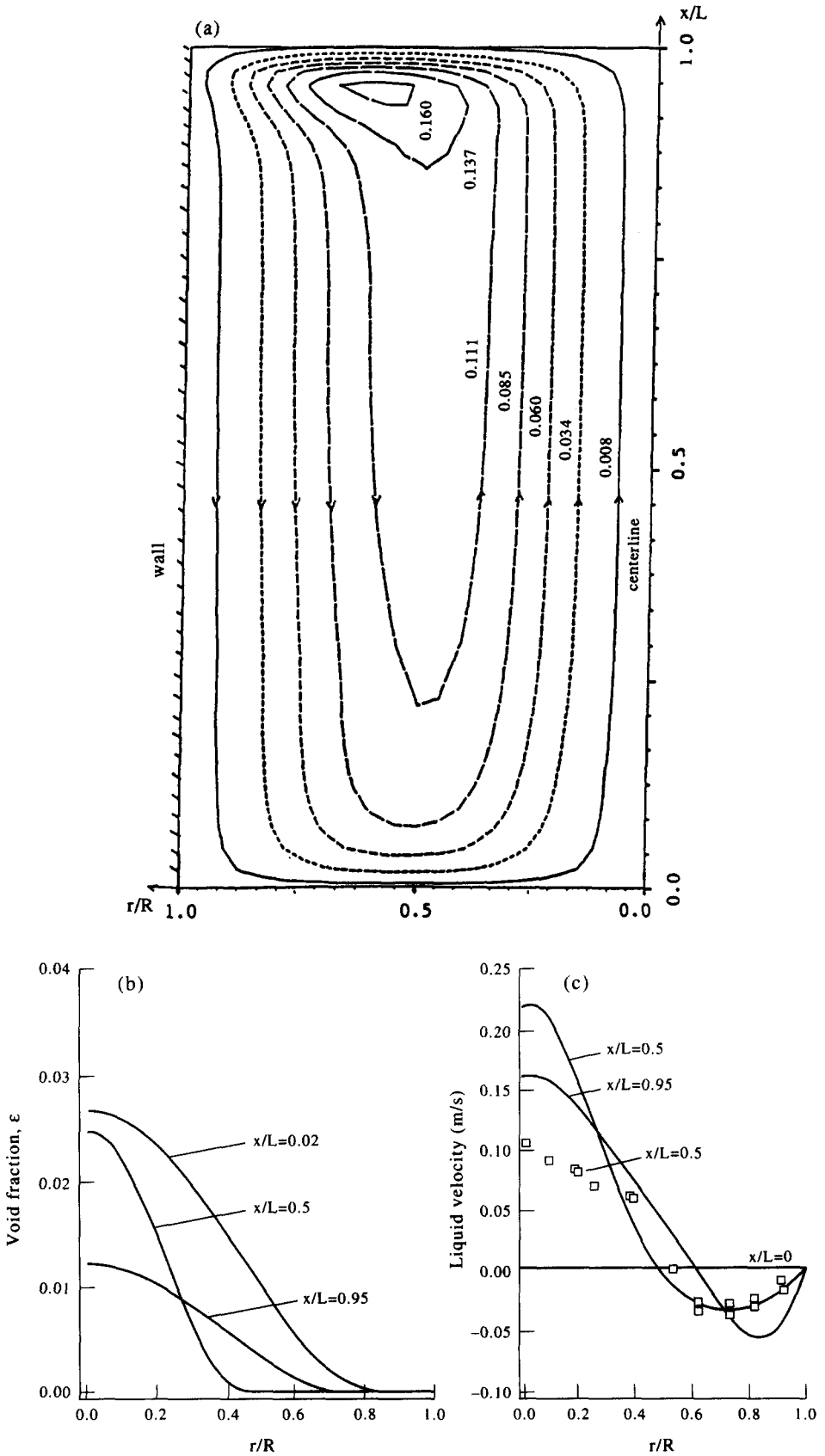

Figure 2. Predictions using a cosine profile for ϵ [12] (experiments by Rietema & Ottengraf 1970). (a) Calculated circulation patterns, (b) calculated ϵ distribution and (c) liquid velocity profiles.

5. RESULTS AND DISCUSSION

Results with prescribed ϵ-profiles

The results of the calculations using a cosine function for the shape of the $\epsilon(r)$ distribution are depicted in figure 2. Here, the experiments of Rietema & Ottengraf (1970) are simulated. The predicted streamlines plotted in figure 2(a) show the commonly observed circulation pattern with a downward flow near the wall and an upward flow near the center of the reactor. The stream function is calculated from

$$\psi = 2\pi \int_0^r (1-\epsilon)\rho_L u_L r \, dr. \qquad [16]$$

The total volume of liquid circulation can be read from figure 2(a) as $Q_{cir} \cong 0.16\ m^3/s$. The center of the circulation zone is predicted to be close to the free surface. As will be discussed later, the circulation pattern is a direct result of the void fraction distribution. The corresponding distribution is shown in Figure 2(b); it should be noted that the shape of the ϵ distribution is assumed, but its magnitude is calculated as part of the solution. Figure 2(b) shows that the centerline value of the void fraction, ϵ_c, decreases with axial distance. This occurs as a result of the increase in the gas velocity towards the free surface; to satisfy continuity [13], as the average value of u_G over the cross section increases the average value of ϵ should decrease. The predicted liquid velocity profiles are shown in figure 2(c). The predicted center line velocity of 22 cm/s, at $x/L = 0.5$ is considerably higher than the measured value of 10.5 cm. The boundary of the reverse flow where $u_L = 0$ is predicted as $r_0 = 0.50$; this is in good agreement with experiments. The agreement is also good for the maximum reverse flow velocities which are seen to be 3–4 and 3–5 cm/s for experiments and predictions, respectively. Of course, these quantities do change with axial distance and with the prescribed bubble street radius, r_s.

Calculations performed with various bubble street radii show that a decrease in r_s causes an increase in ϵ values; thus an increase in the liquid velocity and vice versa. This also effects the boundary of the reverse flow zone. For example, for $r_s/R = 0.65$, the predicted centerline velocity was about 18 cm/s and $r_0/R = 0.52$ at the mid-height of the column. Consequently, the uncertainties in the location of the region where $\epsilon \cong 0$ (i.e. no air bubbles) will cause differences between the experiments and predictions.

The influence of different void fraction profile shapes on the results were also investigated where the gas flow rate and the bubble street diameter were fixed. The linear and parabolic ϵ profiles did not influence the results very much. The reverse flow boundary and the maximum reverse flow velocities were affected the least. The centerline liquid velocity was somewhat higher for the parabolic profile compared to the others. These results show that it is the bubble street diameter and the magnitude of ϵ that primarily affect the flow pattern in a column reactor.

Results from simulation of Rietema & Ottengraf's experiments

In figure 3, the results of the calculations are depicted where ϵ distribution was calculated from [14] directly. The inlet boundary condition was a step function, $\epsilon = \epsilon_0$ for $r_s/R < 0.5$ and $\epsilon = 0$ otherwise. The resulting recirculation pattern shown in figure 3(a) is significantly different from that in figure 2(a). The center of the recirculation zone moved towards the mid-height of the reactor and the total circulated liquid volume flow rate decreased to $Q_{cir} \cong 0.12\ m^3/s$. The corresponding ϵ distribution is shown in figure 3(b). The overall magnitude of ϵ is lower in this case compared to that of figure 2(b), and it does not vary as much in the axial direction [see also figure 3(c)]. On the other hand, the centerline gas velocity first increases and then decreases with the axial distance [figure 3(c)] remaining fairly flat near the mid-height of the column. Figure 3(d) shows that the width of the bubble street prescribed at the inlet first decreases, then remains fairly constant over a large section of the column, finally increases near the top. This is due to the radially inward and outward motion of bubbles near the bottom and near the top, respectively, as a result of convective gas velocities in this direction, and it is in conformity with the usual experimental observations (e.g. Freedman & Davidson 1969). With the predicted ϵ distribution, there is a much closer agreement between the measured and predicted velocity profile at $x/L \cong 0.5$ as shown in figure 3(e). The location of the measurements is reported (Rietema & Ottengraf, 1970) to be near the mid-height of the column. The magnitude of the predicted u_L values are lower because the overall ϵ values are lower and hence less drag force is impacted on the liquid by the gas flow.

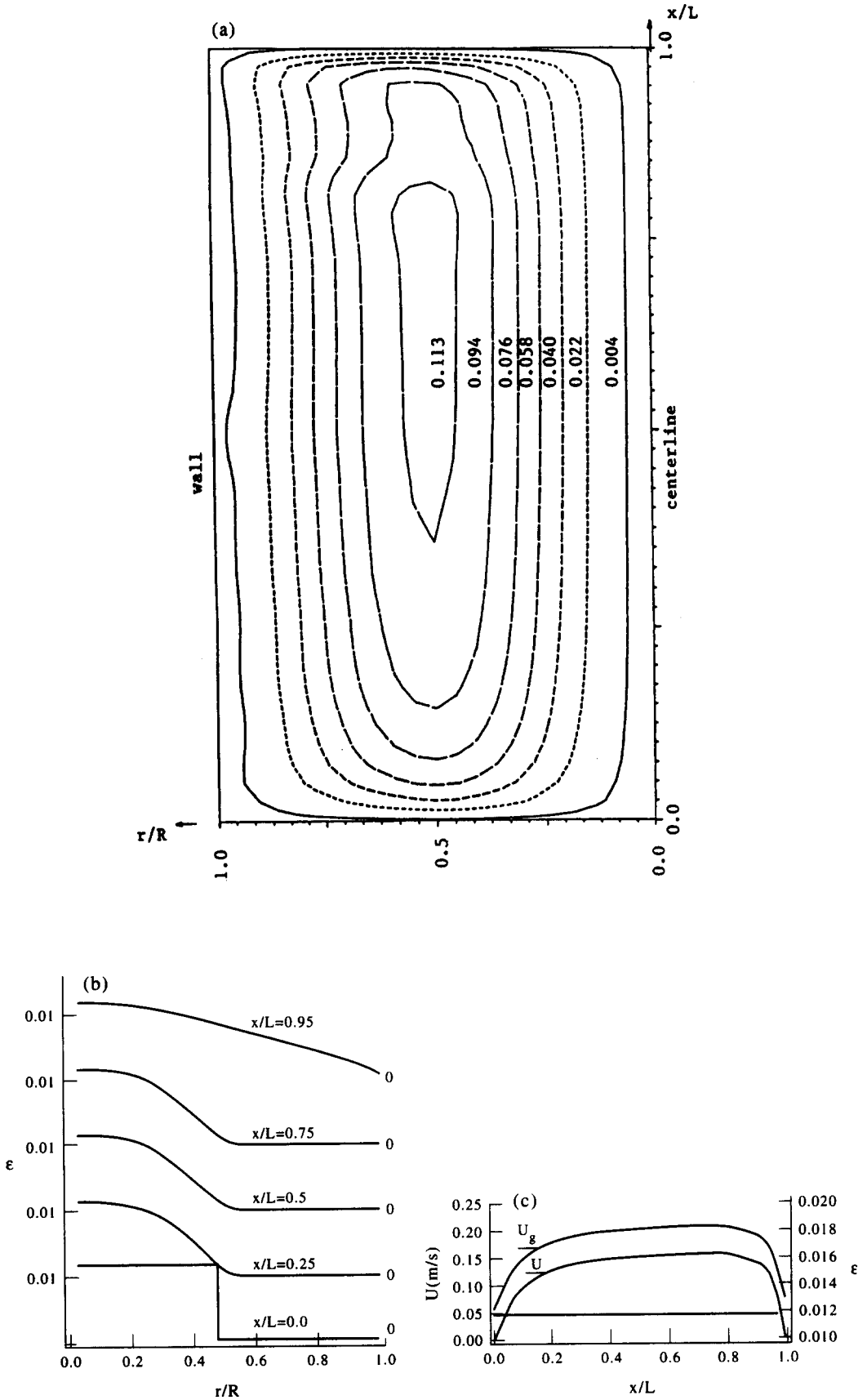

Fig. 3 (a, b and c). *Caption on p. 1064.*

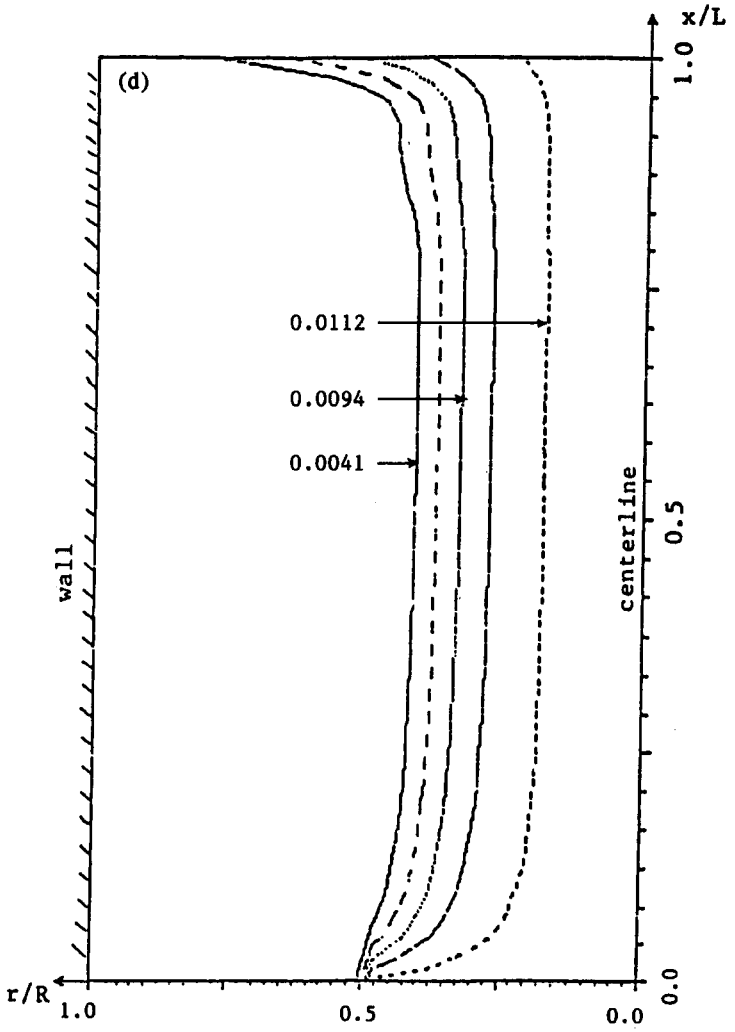

Fig. 3 (d). *Caption overleaf.*

In the present simulations, the migration of bubbles toward the center at the lower half of the column is caused by the inward radical velocity component (i.e. radial convection), the opposite occurs at the upper half of the column. The liquid flow pattern is a direct consequence of the equation of continuity. Initially, bubbles impart a vertical motion on the liquid in the central region (i.e. $\nabla\epsilon \neq 0$). To satisfy continuity, the liquid must form a circulation pattern consisting of one or more large eddies (i.e. circulation cells); the number of these eddies is a function of the aspect ratio of the column. We set the radial relative velocity $v_s = 0$ [7]. This means the bubbles are transported in the radial direction by a convective velocity equal to V_G. The flow pattern in circulation columns is significantly different than the case of fully developed, axisymmetric, two-phase flow investigated by Antal *et al.* (1991). In their case bubble migration may occur as a result of Saffman's lift force (Saffman 1965). Antal *et al.* did include such a force (ironically without referring to Saffman's original paper) but there is a lot of controversy about (even) the direction and magnitude of this force (see e.g. Yamamoto *et al.* 1990 for a review). Another possible mechanism could be the pseudo-turbulence flux terms arising from the non-linear drag correlation equation (see O'Brien *et al.* 1993). For our case the liquid velocities are very small, and the bubbles are concentrated near the region of the column with practically no bubbles near the side walls. Unlike the vertical flow in a tube, initially the liquid is at rest and its motion is derived completely by the motion of bubbles.

The value of the cut-off point ($r_s/R = 0.5$) for the ϵ-step function at $x = 0$ was chosen somewhat arbitrarily. Strictly speaking, this should be the location of the last row of injection holes on the

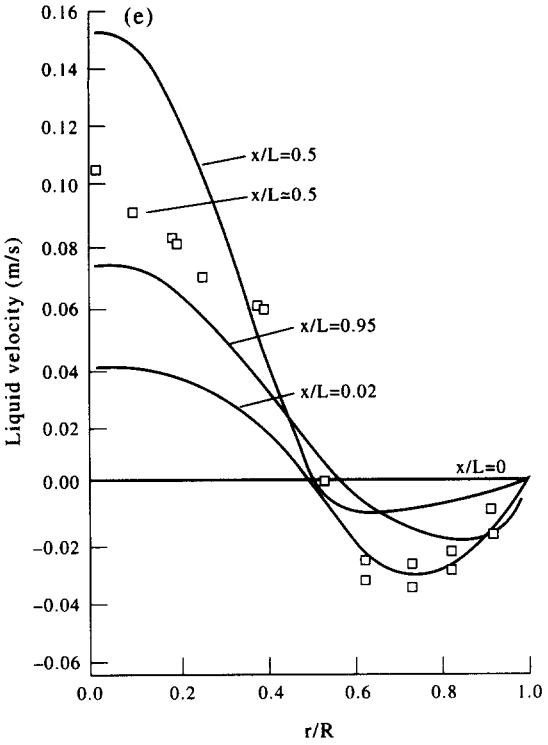

Fig. 3(e)

Figure 3. Predictions with ϵ distribution calculated from the transport equation (experiments by Rietema & Ottengraf 1970). (a) Calculated circulation pattern ($r_s/R = 0.45$), (b) ϵ distribution, (c) liquid velocity, gas velocity and ϵ distribution along the centerline of the column, (d) ϵ contours and (e) liquid velocity profiles.

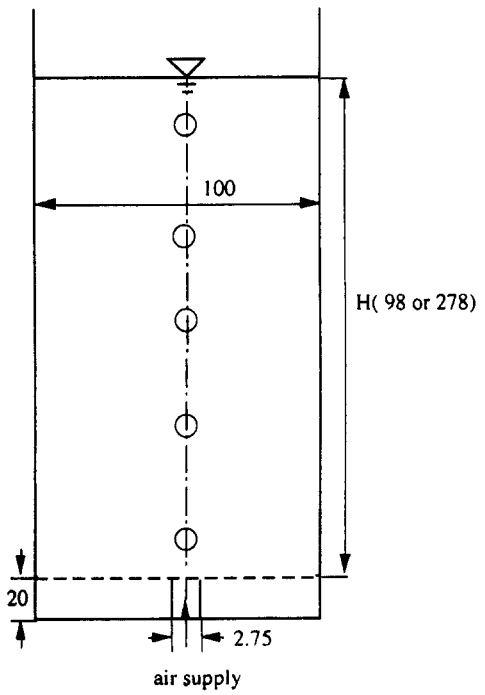

Figure 4. Geometry of the column for a bubble-driven flow investigated by Durst *et al.* (1984). All dimensions are in mm.

distributor plate. A further increase of this parameter to $r_s/R = 0.66$ resulted in much closer agreement between the measured and predicted liquid velocities, but the center of the recirculation zone moved further down towards the inlet. The actual experimental value of r_s/R was pointed out to be 0.543 later by a reviewer. When the air flow was distributed over the whole cross section of the inlet area, the predicted circulation was negligibly small.

This fact seems to have been experimentally verified by Rice (1992) and Rice & Geary (1990), and it opens an interesting discussion on whether there would be any liquid circulation under perfectly symmetric conditions (i.e. no tilting of the column etc.) with uniform ϵ distribution at the inlet. The present calculations indicate that there would be no circulation under such a situation. But the authors believe that this is an unstable flow pattern. The above conclusion should remain valid even if some form of Saffman's lift force is added to the equations, because this force is proportional to the liquid velocity gradient which is initially zero. However, different non-uniform distribution of ϵ at the inlet should result in different circulation patterns, e.g. more than one circulation cell over the vertical span of the column.

Results from simulation of Durst et al.'s experiments

Figure 5 shows the calculated circulation pattern compared to the experimental one for the case of $H = 0.278$ m, the predictions compare favorably with experiments. Figure 6 shows the ϵ

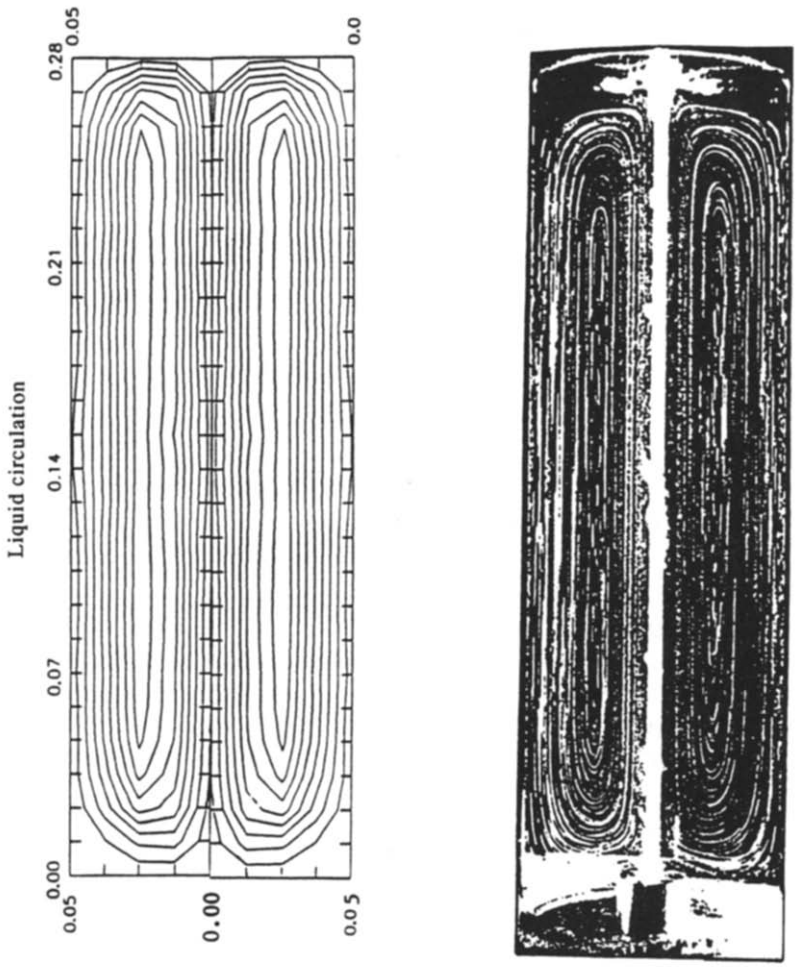

(a) Calculated result **(b) Experimental result**

Figure 5. Calculated circulation patterns; $H = 0.278$ m; experiments by Durst *et al.* (1984).

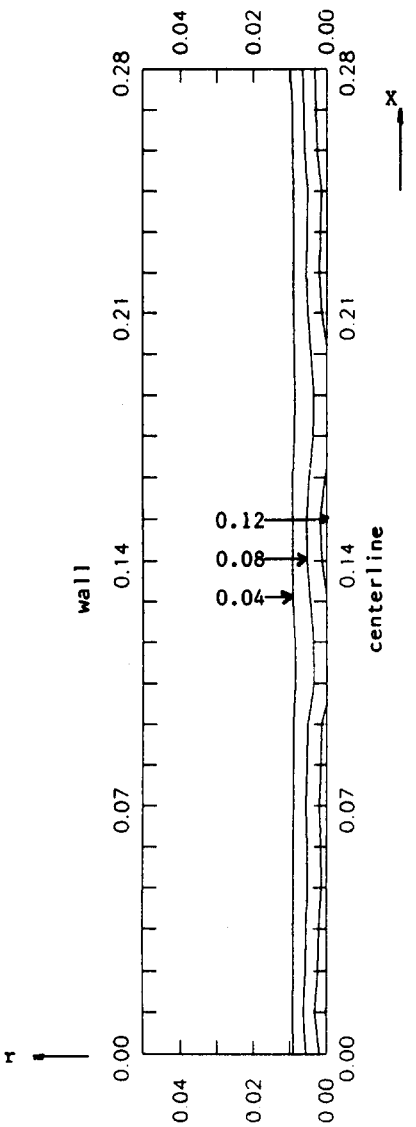

Figure 6. Calculated ϵ contours for Durst *et al.*'s experiments; $H = 0.098$ m.

distribution. There is a narrow region near the center where ϵ values are large and the ϵ profiles remain fairly sharp over the span of the column. This shows that the model predicts the narrow band of bubble street and that the convection in the redial direction is negligibly small.

The calculated liquid velocity profiles for the liquid column height of $H = 0.098$ m are compared with measurements in figures 7 and 8. Here the maximum bubble velocity, $U_{b,max}$ is used for normalization of the liquid velocities. Figure 7(a) depicts the velocity profiles in the lower half of the cylinder, and figure 7(b) depicts those in the upper half of the cylinder. Figure 8(a) and (b) depicts the radial velocity profiles of liquid phase at successive axial locations. It is seen from figure 7 that both the profile shapes and the magnitudes of the axial velocity are predicted in close agreement with measured data except very close to the free surface. The agreement between measurements and predictions is not as good in the case of the redial velocity distributions (figure 8), but the basic features of these profiles are also predicted quite well. The predictions are much better in the lower two-thirds of the column. Near the free surface ($x/H > 0.8$) the predicted peak values of the radial velocity are higher than those from experiments. This discrepancy is most probably due to the assumptions in the loose boundary condition imposed on the radial velocity component at the free surface. The free surface itself was approximated as a plane surface in the calculations. This is not the case in the real situation where rising bubbles disturb the free surface

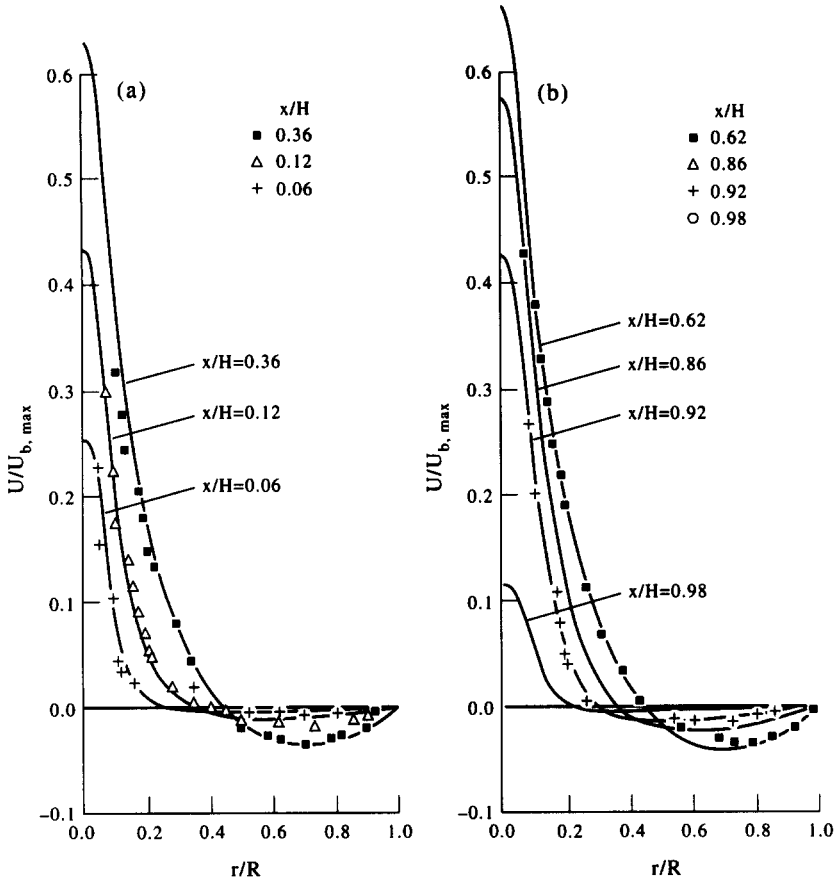

Figure 7. Profiles of axial velocity of liquid phase at various axial stations; $H = 0.098$ m, $U_{b,max} = 3.09$ cm/s. Experiments by Durst *et al.* (1984).

as they leave the liquid column. A better way of handling this boundary could have been to use the kinematic boundary condition and leave the free surface to change according to that equation. Nevertheless, the degree of accuracy with which the overall features of the bubble induced circulation patterns can be predicted with a fairly simple model is noteworthy.

6. CONCLUSIONS

Numerical calculations of the liquid circulation inside on the isothermal column reactor has been performed in two ways: (a) with a prescribed shape for the ϵ profile and (b) with ϵ distribution calculated from the transport equation.

The results indicate that the actual shape of the ϵ profile is not that critical with respect to the circulation patterns and the liquid velocity. The overall magnitude of the void fraction as well as the bubble street diameter seems to be more important. The ϵ profile shapes used in this study, as well as by many other investigators, do not seem to be appropriate for predicting the circulation patterns observed experimentally.

The predictions, including the direct solution for ϵ distribution, lead to a more realistic circulation pattern compared to experimental observations. Hence, the profile assumptions used in previous approximate models should be viewed cautiously. The boundary condition for ϵ at the inlet (i.e. the distributor plate) seems to play a dominant role in determining the overall circulation pattern. At this point numerical investigations need more input from experimental investigations.

The present mathematical model based on the continuum approach and the slip velocity relation also predict reasonably well the overall characteristics of the liquid circulation induced by discrete air bubbles moving along the center line.

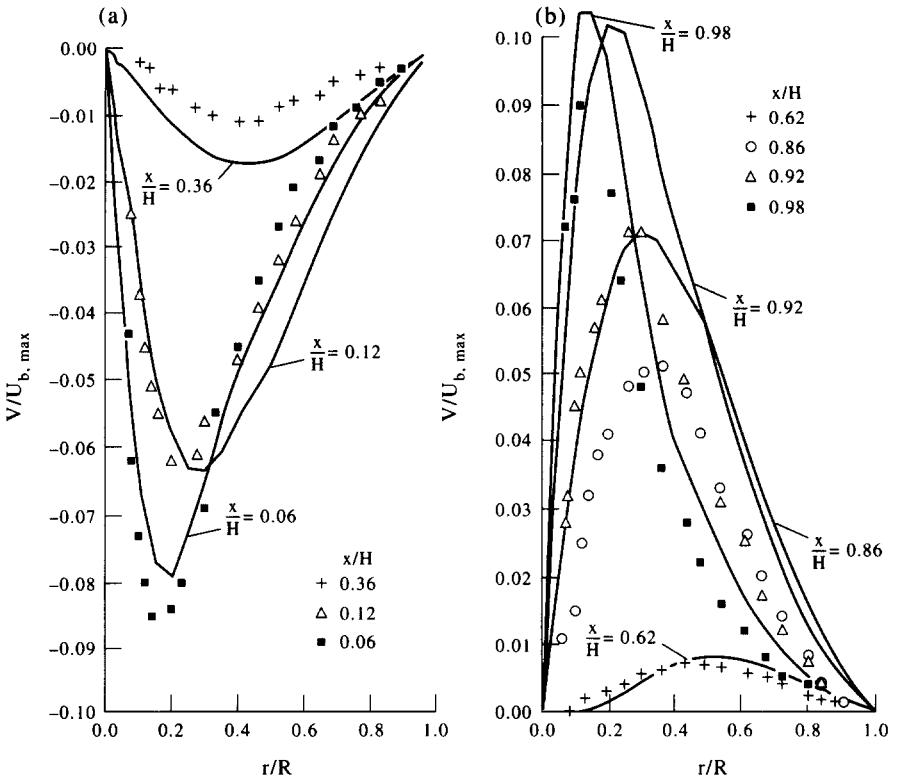

Figure 8. Profiles of radial velocity of liquid phase at various axial stations; $H = 0.098$ m, $U_{b,max} = 3.09$ cm/s. Experiments by Durst *et al.* (1984).

The good agreement of predictions with experiments can be taken as evidence for the validity of the interface momentum exchange function used in the present model.

Future work should include extension to turbulent flow as well as to other flow regimes.

Acknowledgements—This work was supported by the US DOE Pittsburgh Energy Technology Center under Contract No. DE-FG-87PC79935. The calculations were performed on the State of West Virginia Computer Network.

The authors would like to thank Dr Nigel Clark and Dr John Kuhlman for their valuable discussions.

REFERENCES

ANDERSON, T. B. & JACKSON, R. G. 1967 A fluid mechanical description of fluidized beds. *Ind. Engng Chem. Fundam.* **6,** 527–539.

ANTAL, S. P., LAHEY, R. T., JR & FLAHERTY J. E. 1991 Analysis of phase distribution in fully developed laminar bubbly two-phase flow. *Int. J. Multiphase Flow* **17,** 635–652.

CELIK, I. & GEL, A. 1993 Time averaged steady state equations for two-phase flow in fluidized bed reactors. Final Report, US DOE Morgantown Energy Technology Center, Contract No. DE-AP21-G1MC53G42.

CELIK, I. & Y.-Z. WANG 1990 Numerical simulation of liquid circulation in a bubbly column. In *Numerical Methods for Multiphase Flows* (Edited by CELIK, I., HUGHES, D., CROWE, C.T. & LANKFORD, D.). ASME, FED-Vol. 91, pp. 19–26.

CLARK, N. N., ATKINSON, C. M. & FLEMMER, R. L. C. 1987 Turbulent circulation in bubble columns. *AIChE Jl* **33,** 515–518.

CLARK, N., KUHLMAN, J. & CELIK, I. 1990a Circulation in gas–slurry column reactors. Final Report, Mechanical and Aerospace Engineering Dept, West Virginia University, Morgantown, Va. US DOE Pittsburgh Energy Technology Center, Contract No. DE-FG-87PC79935.

CLARK, N. N., VAN EGMOND, J. W. & NEBIOLO, E. P. 1990b The drift-flux model applied to bubble columns and low velocity flows. *Int. J. Multiphase Flow* **16,** 261–279.

CLIFT, R., GRACE, J. R. & WEBER, M. E. 1978 *Bubbles, Drops, and Particles.* Academic Press, New York.

DREW, D. A. 1983 Continuum modeling of two-phase flows. In *Theory of Dispersed Multiphase Flow* (Edited by MEYER, R. E.), pp. 173–190. Academic Press, New York.

DURST, F. & LOY, T. 1984 TEACH: ein Berechnungsverfahren fuer zweidimensionale laminare and turbulente Stroemungen. Report, Institut fuer Hyromechanik, Universtaet Karlsruhe, Karlsruhe, Germany.

DURST, F., TAYLOR, A. M. K. P. & WHITELAW, J. H. 1984 Experimental and numerical investigation of bubble-driven laminar flow in an axisymmetric vessel. *Int. J. Multiphase Flow* **10,** 557–569.

FREEDMAN, W. & DAVIDSON, J. F. 1969 Holdup and liquid circulation in bubble columns. *Trans. Inst. Chem. Engrs* **47,** T251–T262.

GOSMAN, A. D. & IDERIAH, F. J. K. 1976 Teach-2E: a general computer program for two-dimensional, turbulent recirculating flows. Report without number, Dept of Mechanical Engineering, Imperial College, London.

HARLOW, F. H. & AMSDEN, A. A. 1975 Numerical calculation of multiphase fluid flow. *J. Comput. Phys.* **17,** 19–52.

HEWITT, G. F. 1982 Liquid–gas system: void fraction. In *Handbook of Multiphase Systems* (Edited by HETSRONI, G.). Hemisphere, McGraw–Hill, New York.

HILLS, J. H. 1974 Radial non-uniformity of velocity and voidage in a bubble column *Trans. Inst. Chem. Engrs* **52,** 1–9.

HINZE, J. O. 1972 Turbulent fluid and particle interaction. *Prog. Heat Mass Trans.* **6,** 433–452.

HIRT, C. W. 1982 *Numerical Fluid Dynamics. A short course.* Flow Science, Los Alamos, NM.

HOMSY, G. M. 1983 A survey of some results in the mathematical theory of fluidization. In *Theory of Dispersed Multi Phase Flow* (Edited by MEYER, R. E.), pp. 57–70. Academic Press, New York.

JOSHI, J. B. & SHARMA, M. M. 1979 A circulation cell model for bubble columns. *Trans. Inst. Chem. Engrs* **57,** 244–251.

O'BRIEN, T., SYAMLAL, M., NICOLETTI, P. & CELIK, I. 1993 Time-averaged hydrodynamic equations of fluidization, 29th National Heat Transfer Conference, 8–11 August, Atlanta, Ga.

PATANKAR, S. V. 1980 *Numerical Heat Transfer and Fluid Flow.* Hemisphere, New York.

RICE, R. G. & GEARY, N. W. 1990 Prediction of liquid circulation in viscous bubble columns. *AIChE Jl* **36,** 1339–1348.

RICE, R. G. 1992 Private Communication, Dept. of Chemical Engineering, Louisiana State University, Baton Rouge, La.

RIETEMA, K. 1982 Science and technology of dispersed two phase systems. *Chem. Engng Sci.* **37,** 1125–1150.

RIETEMA, K. & OTTENGRAF, S. P. P. 1970 Laminar liquid circulation and bubble street formation in a gas–liquid system. *Trans. Inst. Chem. Engrs* **48,** T54–T62.

SAFFMAN, P. G. 1965 The lift on a small sphere in a slow shear flow. *J. Fluid Mech.* **22,** 385–400.

STEWART, H. B. & WENDROFF, B. 1984 Two-phase flow: models and methods. *J. Comput. Phys.* **56,** 363–409.

WALLIS, G. B. 1962 *Interaction Between Fluids and Particles* (Edited by ROTTENBURG, P. A.). The Institution of Chemical Engineers, London.

WHALLEY, P. B. & DAVIDSON, J. F. 1974 *Proceedings of the Symposium on Multiphase Flow Systems (Symposium Series No. 38),* J5. The Instutution of Chemical Engineers, London.

YAMAMOTO, F., KOUKAWA, M., MONYA, H. & TERAMISHI, A. 1990 Particle lift and drag forces in linear turbulent shear flows. *Proc. 5th Workshop on Two Phase Flow Predictions* (Edited by SOMMERFELD, M. & WENNERBERG, D.), pp. 323–333. Erlargen, Germany.

APPENDIX A

Derivation of Viscous Terms for Two-phase Flow of Incompressible Newtonian Fluids

We consider steady, incompressible, newtonian fluids with constant viscosity. The equations of motion in cartesian tensor notation are:

Continuity

$$\frac{\partial}{\partial x_i}(\rho u_i) = \rho \frac{\partial u_i}{\partial x_i} + u_i \frac{\partial \rho}{\partial x_i} = 0 \qquad [A1]$$

Momentum

$$\rho u_j \frac{\partial u_i}{\partial x_j} = -\epsilon \frac{\partial P}{\partial x_i} + \frac{\partial}{\partial x_j}(\tau_{ij}) + F_i \qquad [A2]$$

(I) (II) (III) (IV)

where macroscopic density $\rho = \rho_G \epsilon$ for the gas phase and $\rho = \rho_L(1-\epsilon)$ for the liquid phase, ϵ is the void fraction, ρ is the pressure, τ is the shear stress tensor and F_i is the phase interaction force. Since the void fraction is not constant, although the fluid has constant microscopic density (i.e. ρ_G = constant, ρ_L = constant), the macroscopic density ρ is not constant, hence $\partial u_i/\partial x_i = \nabla \cdot \mathbf{u} \neq 0$, and the flow is analogous to that of a compressible fluid. The left-hand side of [A2] can be written in conservative form as

$$\frac{\partial}{\partial x_j}(\rho u_j u_i)$$

using [A1].

If we now impose the constitutive equations for a newtonian fluid to model the viscous stresses such that

$$\tau_{ij} = \mu\left(\frac{\partial u_i}{\partial x_j} + \frac{\partial u_j}{\partial x_i}\right) \qquad [A3]$$

and substitute this into [A2] we obtain for the viscous term III

$$\frac{\partial}{\partial x_j}(\tau_{ij}) = \mu \frac{\partial}{\partial x_j}\left(\frac{\partial u_i}{\partial x_j}\right) + \mu \frac{\partial}{\partial x_i}\left(\frac{\partial u_j}{\partial x_j}\right). \qquad [A4]$$

For single-phase incompressible flow

$$\frac{\partial u_i}{\partial x_i} = 0,$$

hence the last term in [A4] vanishes. But this is not the case for two-phase flow (see [A1]). For example, for two-dimensional flow the x-momentum equation (i.e. $i = 1$, $u_1 = u$, $u_2 = v$ in [A4]) will include the following viscous terms

$$\frac{\partial}{\partial x_j}(\tau_{ij}) = \mu\left(\frac{\partial^2 u}{\partial x^2}\right) + \mu\left(\frac{\partial^2 u}{\partial y^2}\right) + \mu\left(\frac{\partial^2 u}{\partial x^2}\right) + \mu\left(\frac{\partial^2 v}{\partial x \partial y}\right). \qquad [A5]$$

The last two terms are the corresponding terms in [2] and [3] in the main text.